Unresolved Sources Naturally Contribute to PeV Gamma-Ray Diffuse Emission Observed by Tibet ASγ

V. Vecchiotti[1,3] , F. Zuccarini[2,3], F. L. Villante[2,3] , and G. Pagliaroli[1,3]
[1] Gran Sasso Science Institute, I-67100 L'Aquila, Italy; giulia.pagliaroli@gssi.it
[2] University of L'Aquila, Physics and Chemistry Department, I-67100 L'Aquila, Italy
[3] INFN, Laboratori Nazionali del Gran Sasso, I-67100 Assergi (AQ), Italy

Abstract

The Tibet ASγ experiment provided the first measurement of the total diffuse gamma-ray emission from the Galactic disk in the sub-PeV energy range. Based on the analysis of TeV sources included in the H.E.S.S. Galactic Plane Survey catalog, we predict the expected contribution of unresolved pulsar-powered sources in the two angular windows of the Galactic plane observed by Tibet ASγ. We show that the sum of this additional diffuse component due to unresolved sources and the truly diffuse emission, due to cosmic-ray interaction with the interstellar medium, well saturates the Tibet data, without the need to introduce a progressive hardening of the cosmic-ray spectrum toward the Galactic center.

1. Introduction

The Tibet ASγ collaboration has recently obtained a measurement of the Galactic diffuse γ-ray emission, providing the first evidence that this component extends to sub-PeV energies (Amenomori et al. 2021). The origin of this high-energy diffuse emission is extensively debated in the very recent literature (see, e.g., Liu & Wang 2021; Koldobskiy et al. 2021; Fang & Murase 2021; Neronov et al. 2021).

An essential step for the interpretation of Tibet ASγ data is the evaluation of the cumulative flux produced by sources that are too faint to be individually resolved. These give rise to a large-scale diffuse emission, superimposed to that produced by cosmic-ray (CR) interactions with the interstellar medium, which can affect the space and energy distribution of the observed signal. Population studies of TeV Galactic sources have shown that unresolved contribution is not negligible in the TeV domain (see, e.g., Cataldo et al. 2020; Steppa & Egberts 2020). Recently Tibet ASγ (Amenomori et al. 2019) and HAWC (Abeysekara et al. 2020) have shown that several Galactic sources produce γ-rays above ∼50 TeV. Moreover, LHAASO-KM2A reports the detection of more than 530 photons at energies above 100 TeV and up to 1.4 PeV from 12 ultra-high-energy γ-ray sources (Cao et al. 2021). It is thus natural to expect that unresolved source contribution may be relevant also in the sub-PeV energy range.

In this paper, we took advantage of the observations provided by H.E.S.S. Galactic Plane Survey (HGPS) in the 1–100 TeV energy domain to discuss the implications of unresolved pulsar-powered sources for the interpretation of Tibet ASγ results. Our approach is based on standard assumptions for the spatial and intrinsic luminosity source distributions (also employed, e.g., Strong 2007; Pothast et al. 2018; Steppa & Egberts 2020). These prescriptions are physically well motivated for a population of sources powered by pulsar activity, like pulsar wind nebulae (PWNe) or TeV

halos, which could represent the dominant component of the TeV sky (as recently suggested by Sudoh et al. 2019; Abdalla et al. 2018a). We show that the inclusion of unresolved contribution from these sources, adding up to standard predictions for CR diffuse flux (Lipari & Vernetto 2018), naturally explains the Tibet ASγ data, without the need to introduce a progressive hardening of the CR spectrum toward the Galactic center.

2. Source Population

It is naturally expected that sources provide a relevant contribution to high-energy γ-ray Galactic emission (see, e.g., Ahlers & Murase 2014, for an estimate of the total emission expected from different classes of Galactic sources). However, the key point is to quantify the fraction of sources that are not resolved by experiments, since these generate a cumulative diffuse emission that adds up to the one produced by CR interactions. The goal of this paper is to predict the unresolved pulsar-powered source contribution to galactic γ-ray emission in the TeV and sub-PeV energy domains. In order to estimate this quantity, we consider the information provided by HGPS in the energy range $1 \, \mathrm{TeV} \leqslant E_\gamma \leqslant 100 \, \mathrm{TeV}$.

We assume that the average source emission spectrum can be described by a power law with an exponential cutoff, i.e., $\varphi(E_\gamma) \propto E_\gamma^{-\beta} \exp(-E_\gamma/E_{\mathrm{cut}})$. The index β is given by the average spectral index of sources included in the HGPS catalog, i.e., $\beta = 2.3$. The cutoff energy is chosen as $E_{\mathrm{cut}} = 500 \, \mathrm{TeV}$. This value is not yet constrained and it corresponds to assuming that the TeV source spectrum observed by H.E.S.S. can be extrapolated with a moderate suppression in the sub-PeV region. In this respect, it is interesting to note that the Tibet ASγ experiment has recently shown that the Crab Nebula emits γ-rays in the sub-PeV region with 5.6σ statistical significance (Amenomori et al. 2019). Moreover, the HAWC experiment has reported evidence of several Galactic sources emitting above ∼50 TeV (Abeysekara et al. 2020) whose γ-ray flux can be described as leptonic emission from electrons/positrons injected with a power-law spectrum and exponential cutoff around 1 PeV (Sudoh et al.

2021). We remark that the adopted value of E_{cut} moderately affects flux predictions for the low energy data points given by Tibet ASγ that are relatively close to the range probed by H.E. S.S. At larger energies ($E_\gamma \geqslant 1$ PeV), the source emission spectrum is limited by photons absorption in the interstellar radiation field (mainly due to cosmic microwave background radiation) that suppresses the flux produced by distant sources. We take this into account, as it is described in Vernetto & Lipari (2016). The source space and luminosity distribution is described by:

$$\frac{dN}{d^3r \, dL_{TeV}} = \rho(\boldsymbol{r}) Y_{TeV}(L_{TeV}) \quad (1)$$

where r indicates the distance from the Galactic center. The function $\rho(\boldsymbol{r})$ is assumed to be proportional to the pulsar distribution parameterized by Lorimer et al. (2006) and to scale as $\exp(-|z|/H)$ with $H = 0.2$ kpc, along the direction z perpendicular to the Galactic plane. It is conventionally normalized to one when integrated into the entire Galaxy.

The function $Y_{TeV}(L_{TeV})$ gives the source intrinsic luminosity distribution in the TeV energy domain.[4] It is parameterized as a power law:

$$Y_{TeV}(L_{TeV}) = \frac{R \, \tau \, (\alpha - 1)}{L_{TeV,Max}} \left(\frac{L_{TeV}}{L_{TeV,Max}} \right)^{-\alpha} \quad (2)$$

in the luminosity range $L_{TeV,Min} \leqslant L_{TeV} \leqslant L_{TeV,Max}$. This distribution is naturally obtained for a population of fading sources, such as PWNe or TeV Halos, created at a constant rate R and having intrinsic luminosity that decreases over a timescale τ according to:

$$L_{TeV}(t) = L_{TeV,Max} \left(1 + \frac{t}{\tau} \right)^{-\gamma} \quad (3)$$

where t indicates the time passed since source formation. In this assumption, the exponent α of the luminosity distribution is given by $\alpha = 1/\gamma + 1$.

The birth rate of PWNe or TeV Halos is similar to that of supernova explosions in our Galaxy, i.e., $R \simeq R_{SN} = 0.019$ yr^{-1} (Diehl et al. 2006). Since γ-ray emission is powered by pulsar activity, the TeV luminosity L_{TeV} is a fraction of the spin-down power $\dot{E}$, i.e., we assume $L_{TeV} = \lambda \dot{E}$ where $\lambda \leqslant 1$. If pulsar energy loss is dominated by magnetic dipole radiation (braking index $n = 3$) and the efficiency of TeV emission does not depend on time ($\lambda \sim$ const), the exponent in Equation (3) is $\gamma = 2$, which corresponds to a source luminosity function $Y_{TeV}(L_{TeV}) \propto L_{TeV}^{-1.5}$. The possibility of λ being correlated to the spin-down power, i.e., $\lambda = \lambda_0 (\dot{E}/\dot{E}_0)^\delta$, was suggested by Abdalla et al. (2018a) that found $L_{TeV} = \lambda \dot{E} \propto \dot{E}^{1+\delta}$ with $1 + \delta = 0.59 \pm 0.21$ by studying a sample of PWNe in the HPGS catalog.[5] In this case, one obtains $\gamma \simeq 1.2$ in Equation (3), which corresponds to a source luminosity function $Y_{TeV}(L_{TeV}) \propto L_{TeV}^{-1.8}$.

---

[4] We indicate with L_{TeV} and Φ_{TeV} the integrated source luminosity and flux and in the energy range 1–100 TeV probed by H.E.S.S.
[5] Our predictions are not sensitive to the absolute value for λ_0 being absorbed inside the parameter $L_{TeV,Max} = \lambda_0 \dot{E}_0$, which we obtain as a best fit from the HGPS data.

3. The Unresolved Source Contribution

In a recent paper (Cataldo et al. 2020), we have shown that H.E.S.S observations can be used to efficiently constrain the TeV source population. In particular, we considered HGPS sources producing a photon flux above 1 TeV larger than 10% of the CRAB flux. Above this threshold, the HGPS catalog can be considered complete (Abdalla et al. 2018b) and it includes 32 sources. We removed from the analysis sources firmly associated with supernova remnants (i.e., Vela Junior, RCW 86, and RX J1713.7-3946) and we treated the residual 29 sources as pulsar powered. This assumption is justified being that this subset is composed of eight firmly identified PWNe, two composite objects showing evidence of both shell and nebular emission, and 19 unidentified sources. In the unidentified subsample, 12 sources have been considered as candidate PWNe in further studies on the basis of new data and/or phenomenological considerations (Wakely & Horan 2008; Abdalla et al. 2018a; Giacinti et al. 2020; Sudoh et al. 2021). The average spectral index of the considered sample of 29 HGPS sources is 2.34 supporting our assumption $\beta = 2.3$.

Namely, by fitting the flux, latitude, and longitude distribution of bright sources in the HGPS catalog, we have obtained $L_{TeV,Max} = 4.9^{+3.0}_{-2.1} \times 10^{35}$ erg s^{-1} and $\tau = 1.8^{+1.5}_{-0.6} \times 10^3$ yr for $\alpha = 1.5$ ($L_{TeV,Max} = 6.8^{+6.7}_{-3.0} \times 10^{35}$ erg s^{-1} and $\tau = 0.5^{+0.4}_{-0.2} \times 10^3$ yr for $\alpha = 1.8$). These results are also valid for extended TeV sources, provided that they have dimensions that do not exceed ~ 40 pc. Moreover, our results are consistent with those obtained by a completely independent analysis of the HGPS catalog performed by Steppa & Egberts (2020). In this paper, we take advantage of the results of Cataldo et al. (2020) to estimate the unresolved flux produced by the considered population in the TeV and sub-PeV energy domains. For definiteness, we take as a reference the case $\alpha = 1.5$. Slightly larger fluxes are obtained for $\alpha = 1.8$.

In order to evaluate the cumulative contribution to diffuse γ-ray signal of sources, which are too faint to be individually detected, we introduce a flux detection threshold Φ_{TeV}^{th} whose value is estimated by considering the performances of the H.E. S.S detector. H.E.S.S is able to resolve point-like sources if they produce an integrated flux Φ_{TeV} in the [1–100] TeV energy domain that is larger than $0.01\Phi_{CRAB}$, where $\Phi_{CRAB} = 2.26 \times 10^{-11}$ cm^{-2} s^{-1} is the flux produced by CRAB in the same energy range. Extended sources can however escape detection even if their flux exceeds this value, as it is understood by looking at the sensitivity curve presented in Figure 13 of Abdalla et al. (2018b). The HGPS catalog can be considered complete for objects producing fluxes larger than $0.1\Phi_{CRAB}$ (with the exception of sources having an angular extension larger than $\sim 1°$ which cannot be observed by H.E.S. S). Taking this into account, we calculate the cumulative emission of unresolved sources as

$$\varphi^{NR}(E_\gamma) = \varphi(E_\gamma) \, \eta(E_\gamma, \Phi_{TeV}^{th})$$
$$\times \int_0^{\Phi_{TeV}^{th}} d\Phi_{TeV} \, \Phi_{TeV} \, \frac{dN}{d\Phi_{TeV}} \quad (4)$$

where $\varphi(E_\gamma)$ is the average source emission spectrum[6]

$$\varphi(E_\gamma) = \frac{1}{K}\left(\frac{E_\gamma}{1 \text{ TeV}}\right)^{-\beta} \qquad (5)$$

and the quantity $dN/d\Phi_{\text{TeV}}$ is the source flux distribution in a given region of the sky (see Equation (A.6) of Cataldo et al. 2020). The function $\eta(E_\gamma, \Phi_{\text{TeV}}^{\text{th}})$ is the average survival probability of photons with energy E_γ emitted by unresolved sources. It includes the gamma absorption due to gamma–gamma interactions on cosmic microwave background photons following the numerical approach described in Lipari & Vernetto (2018). We vary the flux detection threshold in the range $\Phi_{\text{TeV}}^{\text{th}} = [0.01–0.1]\Phi_{\text{CRAB}}$.

Note that the diffuse Galactic γ-ray flux at sub-PeV energies measured by Tibet ASγ is obtained by subtracting/masking the contribution of sources which are included in the TeVCAT catalog (Wakely & Horan 2008). This implies that sources should be faint not only at sub-PeV energies (but also at TeV energies) to escape detection. As a consequence, the above approach which is based on the detection capabilities of experiments operating in the TeV domain is also adequate to investigate unresolved source contribution in the sub-PeV energy range.

4. Results

The flux produced by faint sources which are not individually detected adds up the CR diffuse emission, shaping the radial and spectral behavior of the total diffuse γ-ray flux observed by different experiments. In Figure 1, we show the theoretical predictions for the total diffuse γ-ray flux (green band) as a function of energy in the regions of the Sky probed by the Tibet ASγ experiment (Amenomori et al. 2021). The upper panel (a) refers to the region $25° < l < 100°$, while the lower panel (b) shows the region $50° < l < 200°$; both of them correspond to the latitude range $|b| < 5°$. The unresolved source contribution is obtained as described in the previous section and the thickness of the darker green band corresponds to the uncertainty in the flux detection threshold $\Phi_{\text{TeV}}^{\text{th}}$. Namely, the upper and lower green lines are obtained by assuming $\Phi_{\text{TeV}}^{\text{th}} = 0.1 \Phi_{\text{CRAB}}$ and $\Phi_{\text{TeV}}^{\text{th}} = 0.01 \Phi_{\text{CRAB}}$, respectively. The light green band also includes the uncertainty on this prediction due to the correlated variations of the source population parameters τ and $L_{\text{TeV,Max}}$ within their 1σ uncertainty. The truly diffuse emission, produced by CR interactions with the interstellar gas, is shown by gray solid lines in Figure 1 and corresponds to the "space-independent" model of Lipari & Vernetto (2018). Red data points show the diffuse flux measured by Tibet ASγ. These are obtained after subtracting events within $0°.5$ from known TeV sources included in the TeVCAT catalog (Wakely & Horan 2008). The error bars show 1σ statistical errors. Finally, we also display the CR diffuse flux corresponding to the "space-dependent" model of Lipari & Vernetto (2018) (gray dashed lines) to permit comparison with our predictions. This is obtained by assuming that the CR spectrum in the inner Galaxy is harder than at the Sun position, as it seems to be suggested by Fermi-LAT data (Acero et al.
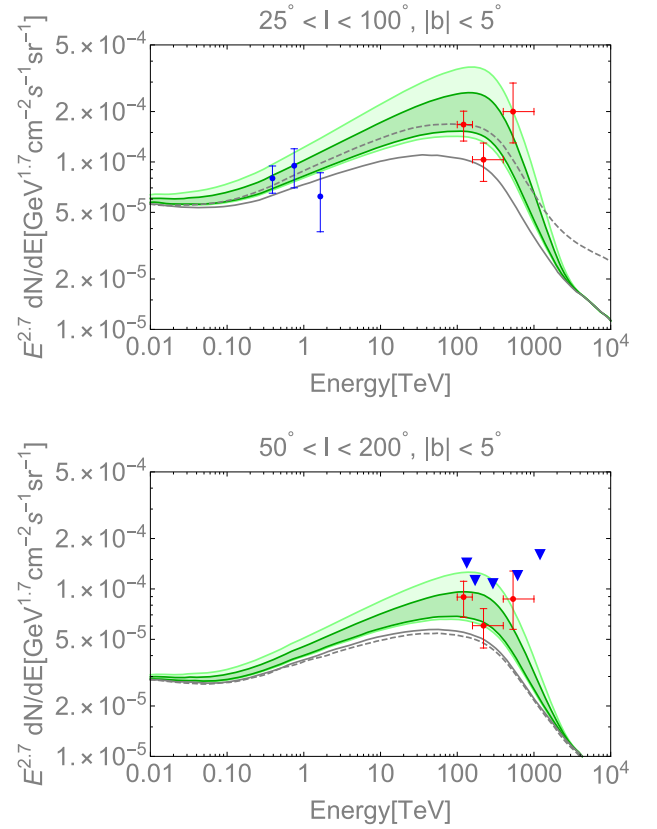

Figure 1. Differential energy spectra of diffuse γ-rays from the Galactic plane in two different angular regions. Red data points are the measurements provided by Tibet (Amenomori et al. 2021). Blue data points in the upper panel are provided by Argo-YBJ (Bartoli et al. 2015), while blue triangles in the lower panel are upper limits by the CASA-MIA experiment (Chantell et al. 1997). Solid and dashed curves display the predicted energy spectra by the space-independent and space-dependent models by Lipari & Vernetto (2018), respectively. The green shaded band represents the total diffuse γ-ray emission obtained by adding the unresolved source contribution estimated in this paper to the γ-ray truly diffuse emission from the space-independent model by Lipari & Vernetto (2018).

2016; Yang et al. 2016; Pothast et al. 2018) (see Peron et al. 2021; Vecchiotti et al. 2021 for alternative explanations).[7]

Several important conclusions can be obtained from Figure 1. First, we see that unresolved source contribution is not negligible for $E_\gamma \geqslant 1$ TeV and becomes progressively more relevant as energy increases as it was also pointed out in Linden & Buckman (2018). This is a natural consequence of the fact that sources are expected to have, on average, a harder spectrum (apart from cutoff effects) than CR diffuse emission. At the energy $E_\gamma \simeq 150$ TeV, corresponding to the first data point of Tibet ASγ, the cumulative flux produced by faint sources is estimated to be 49%–154% (25%–79%) of the truly diffuse signal in the region $25° < l < 100°$ ($50° < l < 200°$).

It is useful to investigate the stability of our results concerning the possibility that some of the 29 sources considered in our analysis turn out to be not pulsar powered. For this purpose, we repeat the fit of the flux, latitude, and longitude distribution of HGPS sources taking into account only the 22 sources with a clear or potential association to

---

[6] The constant K is determined by the condition that $\varphi(E_\gamma)$ is normalized to one when integrated into the $[1–100]$ TeV energy domain, i.e., $K \equiv \int_{1 \text{ TeV}}^{100 \text{ TeV}} dE_\gamma \, \varphi(E_\gamma)$.

[7] The implications of CR spectral hardening in the inner Galaxy have been also discussed in Pagliaroli et al. (2016), Pagliaroli & Villante (2018), and Cataldo et al. (2019) by using a phenomenological approach proposed in Pagliaroli et al. (2016) similar to that adopted by Lipari & Vernetto (2018).
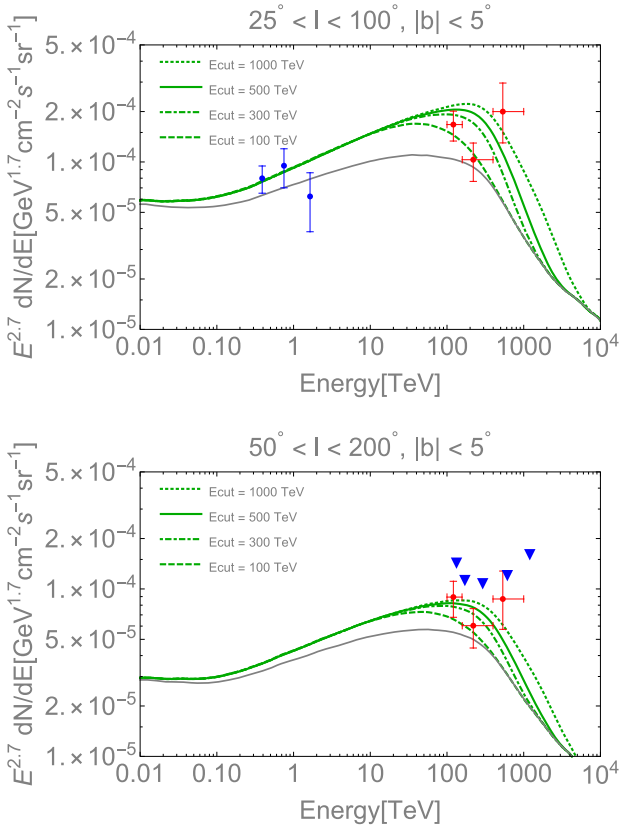
Figure 2. We highlight the role of the assumed energy cut for the sources spectra. The green lines show the differential energy spectra of diffuse γ-rays from the Galactic plane in two different angular regions for an intermediate sensitivity threshold of $\Phi_{TeV}^{th} \sim 0.05\,\Phi_{CRAB}$ and assuming different values for the spectral energy cutoff from 1 PeV to 100 TeV.
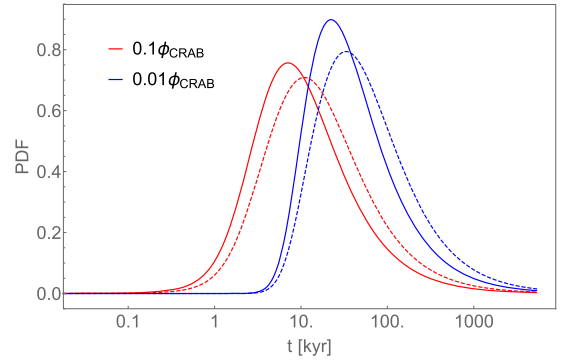

Figure 3. The distribution of sources contributing to unresolved signal as a function of $\log_{10}(t/1\,\mathrm{kyr})$. Thick lines refer to the sky region $|b| < 5°$ and $25° < l < 100°$ while dashed ones refer to the region between $50° < l < 200°$. The blue (red) lines are obtained for $\Phi_{TeV}^{th} = 0.01\Phi_{CRAB}$ ($\Phi_{TeV}^{th} = 0.1\Phi_{CRAB}$).

PWNe. The new best-fit values with this reduced sample are $L_{TeV,Max} = 6.2 \times 10^{35}$ erg s^{-1} and $\tau = 1.1 \times 10^3$ yr. The unresolved flux due to the PWNe population obviously decreases; however, the prediction still falls inside the 1σ statistical uncertainty band reported in light green in Figure 1.

We remark that our prediction is only marginally dependent on the high-energy extrapolation of the source spectra (e.g., the adopted value of the cutoff energy) since the lowest energy data point of the Tibet ASγ experiment nearly overlaps with the energy range probed by H.E.S.S. This is evident in Figure 2 where green lines represent the total diffuse γ-ray emission for intermediate sensitivity threshold $\Phi_{TeV}^{th} \sim 0.05\,\Phi_{CRAB}$, obtained by assuming different values for the spectral energy cutoff from 1 PeV to 100 TeV. In particular, if we assume a lower energy cutoff $E_{cut} = 300$ TeV ($E_{cut} = 100$ TeV), the unresolved source flux at 150 TeV decreases by $\sim 17\%$ ($\sim 68\%$) with respect to the reference case $E_{cut} = 500$ TeV. We can also consider the effects of source spectral index variations (not shown in Figure 2 to avoid overcrowding it). If we take $\beta = 2.4$ ($\beta = 2.5$ TeV), the unresolved source flux at 150 TeV decreases by $\sim 32\%$ ($\sim 54\%$) with respect to the reference assumption $\beta = 2.3$. In all these cases, our predictions for the total diffuse γ-ray emission are still consistent with the first two Tibet data points.

It is interesting to investigate the typical age of sources that give a relevant contribution to an unresolved signal. In Figure 3 we show the relative contribution to unresolved emission as a function of $\log_{10}(t/1\,\mathrm{kyr})$ where t is the age of the source, i.e.,

the time passed since pulsar formation. Thick lines refer to the sky region $|b| < 5°$ and $25° < l < 100°$ while dashed ones refer to the most lateral region between $50° < l < 200°$. With blue lines we show the case of detection threshold $\Phi_{TeV}^{th} = 0.01\Phi_{CRAB}$, corresponding to the lower bound of the green band for the total diffuse flux reported in Figure 3. In this case the dominant contribution is provided by PWNe with an age ranging between $t \sim (22–33)$ kyr, depending on the sky region considered. Red lines correspond to the upper bound of the green band for the total diffuse flux reported in Figure 1 with $\Phi_{TeV}^{th} = 0.1\Phi_{CRAB}$. In this case a younger population provides a dominant contribution peaking between $t \sim (7–11)$ kyr, depending on the sky region considered. The unresolved flux contribution due to sources older than ~ 100 kyr (likely TeV Halos) is expected to be at most 20%.

It is important to remark that our calculations naturally reproduce the Tibet ASγ results both in the low and high longitude observation window, corroborating the conclusion that unresolved PWNe provide a relevant contribution in this energy range. A test of our calculations could be provided by additional observations in the TeV and PeV energy domains. Future experiments with improved sensitivity will be able to resolve more sources in the regions of interest. As an example, CTA, with a sensitivity according to Sudoh et al. (2019), should be able to resolve about 280 (140) pulsar-powered sources in the whole Galaxy, if the typical source size is 10 pc (40 pc).

We also note that the LHAASO-KM2A experiment recently presented preliminary determinations of the diffuse γ-ray signal in the sub-PeV energy domain (Zhao et al. 2021). The LHAASO-KM2A diffuse flux measurement is obtained by masking sources included in the TeVCAT catalog (Wakely & Horan 2008) with a relatively large mask radius.[8] LHAASO-KM2A preliminary data for the longitude window $25° \leqslant l \leqslant 100°$ are lower than Tibet ASγ results and are close to predictions for the space-dependent CR diffuse emission of Lipari & Vernetto (2018). However, they cannot be directly compared with theoretical determinations of the diffuse signal because the masking procedure cuts out a large part of the galactic plane, as is seen in Figure 2 of Zhao et al. (2021), where most of the CR diffuse signal and unresolved emission is

---

[8] The adopted mask radius is $R = 2\sqrt{\sigma_{ext}^2 + \mathrm{p.s.f.}^2}$, where σ_{ext} represents the extension of the source while p. s. f. is the LHAASO-KM2A point-spread-function, and it is typically comparable to or larger than 1° (Zhao et al. 2021).

produced. They thus naturally represent a lower limit to the total diffuse emission.

Finally, by comparing our predictions in panel (a) with the truly diffuse flux given by the space-dependent model of Lipari & Vernetto (2018) (gray dashed lines), we see that the unresolved sources can mimic, at relatively low galactic longitudes, the effects produced by CR spectral hardening in the inner Galaxy (and vice versa). This is in agreement with what we have found in Vecchiotti et al. (2021). By looking at panel (b) we note, however, that the previous statement is not valid in the longitude range $50° \leqslant l \leqslant 200°$ where unresolved sources, different from CR spectral hardening, produce an enhancement of the diffuse emission and provide a good description of the Tibet ASγ data.

The different behavior has a direct explanation. The diffuse emission at $l \geqslant 60°$ is mainly produced, for geometrical reasons, at galactocentric distances comparable to or larger than the distance of the Sun from the Galactic center. As a consequence, it is not sensitive to variations of the CR distribution in the inner Galaxy. On the contrary, it can be increased by unresolved sources, which are distributed in the whole Galaxy, and thus produce a nonvanishing contribution even at large latitudes. We remark that this point is important because it provides the possibility to distinguish between the two effects in present and future experiments. At the moment, the inclusion of unresolved PWNe contribution produces a better description of the Tibet ASγ data than CR spectral hardening.

ORCID iDs

V. Vecchiotti ⓘ https://orcid.org/0000-0002-9802-3678

F. L. Villante ⓘ https://orcid.org/0000-0001-7667-4499
G. Pagliaroli ⓘ https://orcid.org/0000-0002-6751-9996

References

Abdalla, H., Abramowski, A., Aharonian, F., et al. 2018a, A&A, 612, A2
Abdalla, H., Abramowski, A., Aharonian, F., et al. 2018b, A&A, 612, A1
Abeysekara, A. U., Albert, A., Alfaro, R., et al. 2020, PhRvL, 124, 021102
Acero, F., Ackermann, M., Ajello, M., et al. 2016, ApJS, 223, 26
Ahlers, M., & Murase, K. 2014, PhRvD, 90, 023010
Amenomori, M., Bao, Y. W., Bi, X. J., et al. 2019, PhRvL, 123, 051101
Amenomori, M., Bao, Y., Bi, X. J., et al. 2021, PhRvL, 126, 141101
Bartoli, B., Bernardini, P., Bi, X. J., et al. 2015, ApJ, 806, 20
Cao, Z., Aharonian, F. A., An, Q., et al. 2021, Natur, 594, 33
Cataldo, M., Pagliaroli, G., Vecchiotti, V., & Villante, F. L. 2019, JCAP, 12, 050
Cataldo, M., Pagliaroli, G., Vecchiotti, V., & Villante, F. L. 2020, ApJ, 904, 85
Chantell, M. C., Covault, C. E., Cronin, J. W., et al. 1997, PhRvL, 79, 1805
Diehl, R., Halloin, H., Kretschmer, K., et al. 2006, Natur, 439, 45
Fang, K., & Murase, K. 2021, ApJ, 919, 93
Giacinti, G., Mitchell, A. M. W., López-Coto, R., et al. 2020, A&A, 636, A113
Koldobskiy, S., Neronov, A., & Semikoz, D. 2021, PhRvD, 104, 043010
Linden, T., & Buckman, B. J. 2018, PhRvL, 120, 121101
Lipari, P., & Vernetto, S. 2018, PhRvD, 98, 043003
Liu, R.-Y., & Wang, X.-Y. 2021, ApJL, 914, L7
Lorimer, D. R., Faulkner, A. J., Lyne, A. G., et al. 2006, MNRAS, 372, 777
Neronov, A., Semikoz, D., & Vovk, I. 2021, A&A, 653, L4
Pagliaroli, G., Evoli, C., & Villante, F. L. 2016, JCAP, 11, 004
Pagliaroli, G., & Villante, F. L. 2018, JCAP, 08, 035
Peron, G., Aharonian, F., Casanova, S., Yang, R., & Zanin, R. 2021, ApJL, 907, L11
Pothast, M., Gaggero, D., Storm, E., & Weniger, C. 2018, JCAP, 10, 045
Steppa, C., & Egberts, K. 2020, A&A, 643, A137
Strong, A. W. 2007, Ap&SS, 309, 35
Sudoh, T., Linden, T., & Beacom, J. F. 2019, PhRvD, 100, 043016
Sudoh, T., Linden, T., & Hooper, D. 2021, JCAP, 08, 010
Vecchiotti, V., Pagliaroli, G., & Villante, F. L. 2021, NatCo, submitted (10.21203/rs.3.rs-539249/v1)
Vernetto, S., & Lipari, P. 2016, PhRvD, 94, 063009
Wakely, S. P., & Horan, D. 2008, Proc. ICRC (Mérida), 3, 1341
Yang, R., Aharonian, F., & Evoli, C. 2016, PhRvD, 93, 123007
Zhao, S., Zhang, R., Zhang, Y., & Yuan, Q. 2021, Proc. ICRC (Berlin), ICRC2021, 859